Reactive Coaxial Electrospinning of ZrP/ZrO2 Nanofibres

Journal Name

ARTICLE TYPE

Reactive Coaxial Electrospinning of ZrP/ZrO$_2$ Nanofibres

S. Subianto*[a], A. Donnadio[b], S. Cavaliere[a], M. Pica[b], M. Casciola[b], D. J. Jones*[a], and J. Rozière[a]

5 Zirconium phosphate/zirconium oxide nanofibres have been fabricated using a novel, reactive coaxial electrospinning approach. In this approach, a zirconium precursor and a phosphorus source are spun together from separate solutions, using a coaxial needle, in order to delay formation of zirconium phosphate gel. Reaction between the zirconium and phosphorus sources is considered to initiate at the interface region in the coaxial fibres. The resultant nanofibres are calcined and further treated with
10 H$_3$PO$_4$. The formation of ZrP/ZrO$_2$ nanofibres was confirmed using ^{31}P MAS NMR. Electron microscopy shows the fibre morphology to depend on solution parameters, and that the X-ray amorphous fibres exhibit compositional homogeneity. Incorporation of the nanofibres into the short-side-chain perfluorosulfonic acid ionomer Aquivion™ yields membranes having significantly increased mechanical properties with greater elastic modulus and yield point as well as increased proton conductivity compared
15 to both cast and commercial Aquivion™ membrane.

Introduction

Zirconium phosphate (ZrP) has been investigated as filler material for fuel cell membranes as it is a good proton conductor that is chemically and thermally stable. Several studies that have
20 investigated the use of ZrP nanoparticles in composite membranes with Nafion®[1-4] have shown improved mechanical properties or proton conductivity above 100 °C, while also reducing methanol crossover in direct methanol fuel cell applications.

25 However, in order to improve the performance of such composites, it is important to control not only the physical properties of the ZrP, but also its morphology in order to optimise its interaction with the polymer matrix. In this regard, previous
30 studies on ZrP composites have used only nanoparticles[5, 6] and no studies have investigated other morphologies such as nanofibres, which may provide stronger interaction and greater reinforcing effect. Unlike lanthanide phosphates which may form nanowires[7] due to their crystal structure, zirconium phosphate has a layered
35 structure, and since its macroscopic morphology can be considered to derive from its crystal structure, fibre-form ZrP has not been reported yet. But in the macroscale, the use of nanofibres rather than nanoparticles in a composite membrane could provide several advantages in terms of reinforcing effect as
40 the fibre length and high aspect ratio provide an extended interaction with the proton conducting matrix[8].

Electrospinning is attracting significant interest for the fabrication of inorganic nanofibres due to its versatility, reproducibility, and
45 the possibility of obtaining a mechanically robust mat of nanofibres[9]. There are several approaches that have been used to electrospin inorganic nanofibres. In certain cases, materials such as cesium dihydrogen phosphate[10, 11] which forms long chains of condensed phosphates may be electrospun directly[12]. A more
50 commonly used approach is that pre-formed inorganic particles

are electrospun using the aid of a carrier polymer[13]. In another approach, a precursor solution or a nanoparticle dispersion is electrospun into fibres with the aid of a carrier polymer[14], and inorganic fibres are obtained after thermal treatment in air to
55 remove solvents and the carrier polymer. In previous studies, electrospun ZrO$_2$ fibres have been obtained[15-17], however direct electrospinning of ZrP nanofibres from precursor solutions has not been reported.

60 We describe here a novel method to fabricate ZrP nanofibres by reactive coaxial electrospinning. Coaxial electrospinning uses a coaxial needle with a core and a sheath solution, which allows the co-electrospinning of separate precursor solutions leading to the introduction of the phosphorus source into the fibre with a
65 potential for ZrP formation during the electrospinning process while keeping the carrier polymer concentration to a minimum.. Through post-synthesis treatment, a ZrO$_2$/ZrP nanofibre mat is obtained.

Experimental

70 ### Materials

Zirconyl propionate (ZrO$_{1.26}$(C$_2$H$_5$COO)$_{1.49}$, MW = 220 Da) was supplied by MEL Chemicals, England. Polyvinyl pyrrolidone (PVP, m.w. 1,000,000), P$_2$O$_5$, 1-propanol, and H$_3$PO$_4$ (solid, crystalline) were purchased from Aldrich and used as received. A
75 20 wt % Aquivion™ dispersion in water (D70-20B, ionomer equivalent weight = 700 g/eq) was kindly supplied by Solvay Specialty Polymers, Italy. Coaxial electrospinning was carried out using a coaxial needle and a rotating drum setup purchased from Linari Biomedical combined with a syringe pump (KP
80 Scientific) and high voltage power supply (Spellman HV). For electrospinning, the required quantity of zirconyl propionate and PVP were dissolved in 1-propanol to make the solution spun as the "core" (10 % w/v zirconyl propionate, 7 % w/v PVP), while the solution spun as the "sheath" (10 % w/v P$_2$O$_5$) was prepared

by dissolving the required quantity of P_2O_5 in 1-propanol.

Reactive coaxial electrospinning of ZrP/ZrO₂ nanofibres

The core and sheath solutions were loaded into two separate syringes and mounted on separate syringe pumps in order to
5 allow separate flow rates for the two solutions. The syringes were connected to the coaxial needle via fluorinated ethylene propylene (FEP) tubing and luer lock adapters. In a typical experiment, electrospinning was carried out using the following parameters: applied potential of 12 kV, needle-collector distance
10 of 8 cm, a core solution flow rate of 0.24 ml/h, and a shell solution flow rate of 0.08 mL/h. A rotating drum collector was used (with a 50 mm drum diameter) utilising a drum rotational speed of 800 rpm and a drum translational speed of 10 mm/s. The needle was cleaned regularly during deposition to prevent the
15 build up of ZrP gel. After a sufficient quantity of material was deposited on the drum, the nanofibre mat was removed and calcined at 450 °C, then treated in 0.2 M H_3PO_4 in 1-propanol at 80 °C overnight and then rinsed several times with 1-propanol. The materials were then dried at 80 °C.

20 ### Preparation of ZrP/ZrO₂ nanofibres and the Aquivion™/ZrP composite membranes

Composite membranes of ZrP/ZrO₂ nanofibres and Aquivion™ were fabricated by mixing the appropriate quantity of ZrP/ZrO₂ nanofibres in a 5 % dispersion of Aquivion™ in 1-propanol. The
25 mixture was then sonicated until a homogeneous dispersion is obtained, and cast using the doctor blade method. The cast membrane was then dried at room temperature overnight before thermal treatment at 160°C for 1 hour.

Characterisation of ZrP/ZrO₂ nanofibres and
30 ### Aquivion™/ZrP composite membranes

The nanofibre morphology was analysed by SEM using a Hitachi S-4800 scanning electron microscope. Data analysis and size distribution was performed using ImageJ image processing software. ^{31}P MAS NMR spectra were recorded on a Varian
35 VNMRS 400 MHz spectrometer with a 1.6 mm Varian T3 probe. The spectra were recorded using a single pulse sequence with samples spinning at 40 kHz, a $\pi/6$ pulse of 2 μs and 200 s recycling delay. The morphology of the membrane was observed by cross-section TEM using a JEOL JEM - 2200FS HRTEM
40 equipped with energy-dispersive spectroscopy analysis (EDS). The samples were embedded in resin and cured at 80 °C and microtomed using a Reichert ultramicrotome, with the sample being cut into sections of ca 80-100 nm thickness and deposited on copper grids for TEM. Mechanical tensile strength
45 measurements were carried out on a Zwick Roell Z1.0 static material testing machines equipped with a 200N static load cell and a controlled temperature/humidity chamber and the data were analysed with a TestXpert V11.0 software. The specimen was cut using a die to a size of 90 x 5 mm and the displacement speed
50 was 2 mm.min^{-1}. The in-plane conductivity of the membranes was determined on 50 x 5 mm strips in the frequency range 10 Hz – 100 kHz, at 100 mV signal amplitude by four-probe impedance measurements using an Autolab PGSTAT30 potentiostat/galvanostat equipped with an FRA module.

55

Results and Discussion

Electrospinning of ZrP/ZrO₂ nanofibres

Previous studies on the electrospinning of inorganic nanofibres, generally oxides, have involved the use of a carrier polymer that
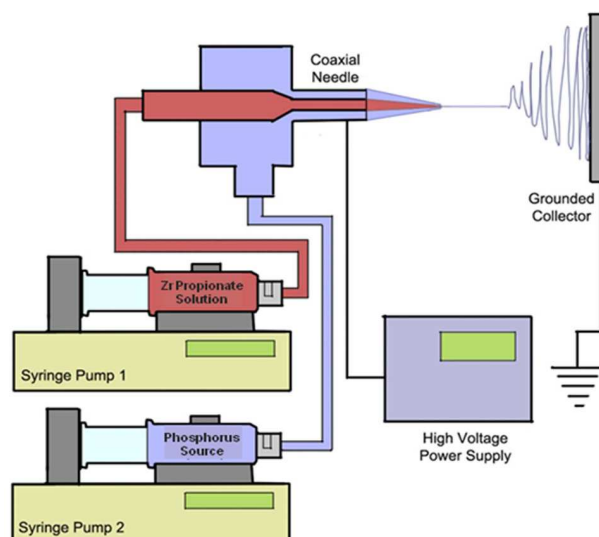
60 **Scheme 1** 'Reactive' coaxial electrospinning of ZrP/ZrO₂ fibres

is subsequently removed by calcination[14]. However, this method is not applicable to nanosized ZrP, as ZrP nanoparticles forms a gel that is unsuitable for direct electrospinning. Studies by Carriere et al[18, 19] have shown that post-treatment of ZrO₂
65 nanoparticles with phosphoric acid[20] can yield a covalently bound surface layer of ZrP. Although this method could be applied to electrospun ZrO₂ nanofibres, it is likely that only a thin surface coating of ZrP would result.

70 To overcome this limitation, we have developed a method based on coaxial electrospinning whereby the shell and core solutions contain the sources of phosphorus and zirconium respectively,,resulting in a 'reactive' electrospinning where ZrP is formed in situ during fibre formation (Scheme 1). In this method,
75 phosphorus pentoxide (P_2O_5) was used as the phosphorus source, since it has the advantage of presenting a slower gelling time when the solution of P_2O_5 comes into contact with the Zr precursor solution, than is observed using H_3PO_4 thus enabling a short time period during which the solution is electrospinnable.
80 Indeed, our initial attempts at single needle electrospinning observed this short induction period where electrospinning of the solution is possible before the solution gels due to the formation of ZrP through the hydrolysis of P_2O_5 with moisture in the atmosphere, and reaction with zirconyl propionate. This problem
85 is overcome through the use of coaxial electrospinning as the two solutions are kept separate until they exit the needle, allowing fibre formation before the ZrP gel formation. As such, the produced nanofibres would contain a mixture of unreacted Zr precursor and alkyl-terminated ZrP species formed as the P_2O_5
90 reacted with the alcohol solvent to form alkyl phosphate species which in turns reacted with the Zr precursor. Calcination was performed in air afterwards in order to convert the unreacted Zr precursor in the fibres into ZrO₂ and also remove the carrier polymer.

95

The fibre formation depends significantly on the solution parameters, and is generally impeded by premature ZrP formation. In this study, the mass ratio between Zr precursor: P_2O_5 was kept at 3:1 or greater in order to prevent gelling of the
100 solution during electrospinning, which results in large droplets being formed rather than fibres. The resultant mat shows fibres of
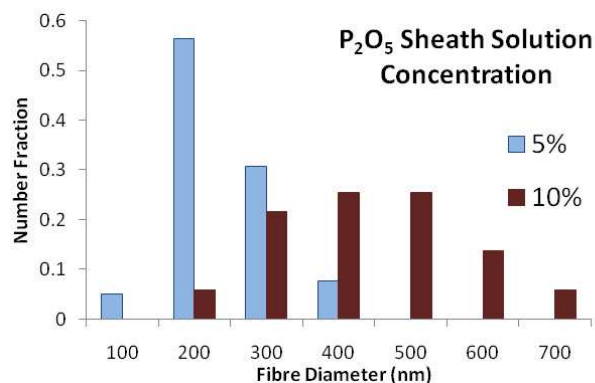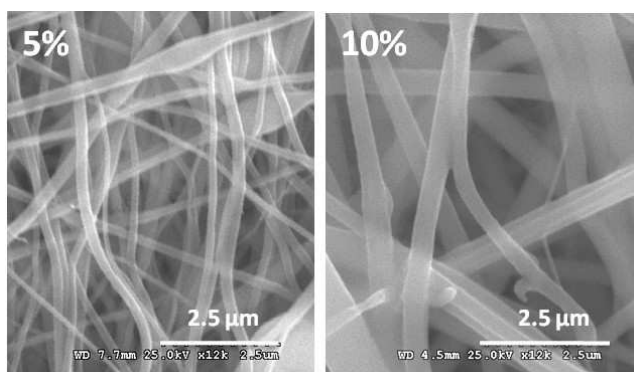
Fig. 1 SEM images and fibre size distribution of electrospun ZrP fibres (prior to calcination) spun using a Zr Propionate: P_2O_5 mass ratio of 4:1 (which was kept constant by modifying the sheath solution flow rate) and a sheath solution concentration of 5 % and 10 % w/v P_2O_5.

5

100-600 nm diameter, which is affected principally by the concentration of the P_2O_5 sheath solution (Figure 1). At lower P_2O_5 solution concentration, the fibre size distribution did not change significantly with the Zr precursor: P_2O_5 mass ratio, and
10 only when the P_2O_5 solution concentration was increased did the effect become observable at Zr precursor: P_2O_5 mass ratio below 4:1. This is attributed to two factors, one is that higher P_2O_5 concentration would result in a more rapid gelling of the fibres, resulting in a larger fibre diameter. The second factor at play is
15 the 'solvent-sheath' effect, in that studies using coaxial electrospinning[21, 22] have found that having a solvent as the sheath solution slows down the evaporation of solvent during electrospinning and resulted in finer fibres. However, in the case of our reactive electrospinning of ZrP, the gelling effect
20 predominates, and as such the lowest Zr precursor : P_2O_5 mass ratio obtainable was 3:1, which still produces fibres whereas ratios below this value results in gelling of the solution as they exit the needle, impeding the electrospinning process.

25 After calcination, the fibre diameter decreased significantly, with a reduction in average fibre diameter from 420 to 220 nm for samples prepared with a Zr precursor/ P_2O_5 mass ratio of 4/1 (Figure 2). The calcined fibre mats were brittle and still possess a slightly brown colouration, indicating the presence of
30 carbonaceous material. TEM cross section of the fibre (Figure 3) shows that the material is porous and granular, without a distinction between the surface area and the inner core. HRTEM EDS analysis (results shown in Table 1) also indicates that the ZrP content of the fibres remain the same throughout, which is
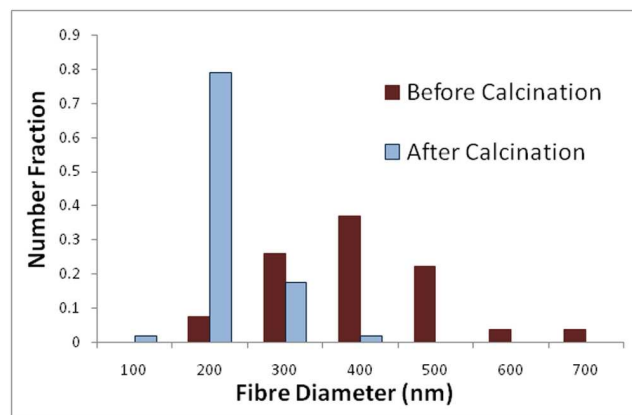35 attributed to the rapid

Fig. 2 Fibre size distribution of distribution of electrospun ZrP fibres before and after calcination; Fibres were electrospun using a Zr Propionate: P_2O_5 mass ratio of 4:1 and a sheath solution concentration of 10 % w/v P_2O_5.
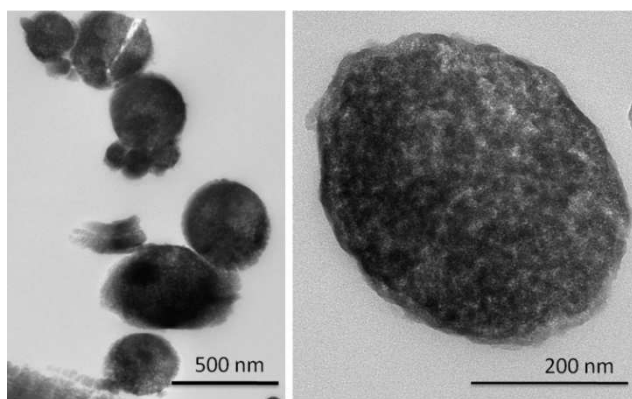

40

Fig. 3 TEM Cross section micrograph of the ZrP/ZrO$_2$ fibres

Table 1 HRTEM EDS Analysis of the Zr and P content of the centre and surface of the ZrP/ZrO$_2$ fibres cross section.

Sampling Site	Mol % Zr	Mol % P
Centre	36	47
Surface	39	48

45 formation of ZrP which formed this amorphous morphology coupled with the carrier polymer, the removal of which (through calcination) may have resulted in the porous, loose-grain morphology observed. The molar ratio of Zr:P was also similar to what was expected based on the mass ratio of the precursors (4:1
50 mass ratio of Zirconyl Propionate to Phosphorus Pentoxide), which translates to a 3:4 molar ratio of Zr to P. This was greater than what would be expected for ZrP (a 1:2 theoretical molar ratio of Zr:P), which indicates the presence of ZrO$_2$ in the fibres.

55 This was supported by Wavelength Dispersive X-Ray Spectroscopy results (See Supporting Information) which shows a random distribution of zirconium, phosphorus, and oxygen throughout the cross section of the fibres, indicating a random distribution of ZrP and ZrO$_2$ within the fibres. The amorphous
60 nature of the fibres was also confirmed by XRD which did not show any peak for crystalline ZrP, indicating that the ZrP present in the fibres are completely amorphous. In contrast, the XRD spectra (see Supporting Information) show peaks that can be attributed to orthorhombic zirconia (JCPDS 00-034-1084),
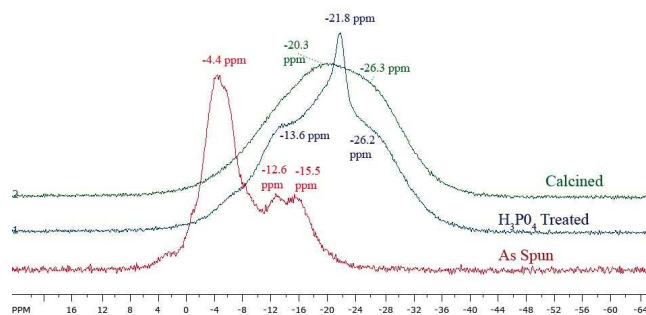65 confirming the presence of ZrO$_2$ in the fibres.

Fig. 4 Solid state MAS ^{31}P NMR spectra of the ZrP nanofibres: as electrospun, after calcination, and after treatment with H_3PO_4.

Solid state MAS ^{31}P NMR experiment was performed in order to study the ZrP formation in the fibres. In the literature, the chemical shift of the main peak in crystalline α-ZrP is measured at -20 ppm[23], while amorphous ZrP shows a main peak at -23 ppm[2]. NMR spectra of ZrP shows multiple peaks due to the
[10] different connectivities of the phosphate. This can be denoted using the Q notation, with Q^n where n is the number of Zirconium metal centres connected to the phosphate via an oxygen bridge (HO-P-O-Zr). In amorphous α-ZrP, the main peak at -23 pppm is due to Q^3 phosphate, while the chemical shift for Q^0 to Q^4
[15] phosphates has been reported as -0.7, -7.9, -15.3, -22.6, and -28.8 ppm respectively[24].

After electrospinning, the ^{31}P NMR analysis of the nanofibres (Figure 4) shows overlapping peaks around 0 to -15 ppm with
[20] three main peaks at –4.4, -12.6, and -15.5 ppm which indicates that the as-spun mat contains alkyl phosphate species due to the solvent used, however the main peak at –4.4 ppm is most likely due to alkyl-terminated, Q^1 phosphate species due to the reaction between the alkyl phosphate formed from P_2O_5 and the alcohol
[25] solvent[25] and the zirconium precursor. The lack of a peak at zero due to phosphoric acid indicates that most of the available phosphorus reacted immediately, and little unreacted P_2O_5 remained to react with moisture in the atmosphere to form phosphoric acid. Thus, the smaller peaks at -12.6 and -15.5 ppm
[30] may be attributed to alkyl- terminated species rather than the OH-terminated zirconium hydrogenphosphate ($Zr(HPO_4)_2$). Both these peaks have been previously reported as corresponding to Q^2 phosphate species, and although the exact nature of the species giving rise to each is unclear it may be due to the amorphous
[35] form of ZrP. There is only a very small shoulder at around -23 ppm, which indicates that at this stage that OH terminated, Q^3 $Zr(HPO_4)_2$ has not yet been formed and the dominant phosphate species is probably a mixture of alkyl-terminated phosphates.

[40] After calcination, the ^{31}P NMR shows a very broad peak centred around -20 ppm. This indicates that at this stage, ZrP has been formed, however it is in a mixed form containing various coordination which may include pyrophosphate (ZrP_2O_7) species containing P-O-P bonds. Acid treatment was necessary to convert
[45] this into ZrP, and after acid treatment the NMR spectra resembles that of amorphous zirconium hydrogenphosphate reported by Hudson et al[24]. The peak at -21.8 ppm becomes sharper, indicating the conversion of the phosphate species into zirconium hydrogenphosphate species through the breaking of the P-O-P
[50] bonds in the zirconium pyrophosphate species and creating the

Table 2 Proton conductivity measurement of the composite membranes compared to reference membranes.

Membrane Sample	T (°C)	RH (%)	σ_{ip} (mS.cm^{-1})
Commercial, extruded EW790 Aquivion™	80	50	59
		90	190
	110	50	56
		90	210
Cast EW700 Aquivion™	80	50	62
		90	230
	110	50	78
		90	294
Cast EW700 Aquivion™, 5 % ZrP nanofibres	80	50	77
		90	270
	110	50	99
		90	330
Cast EW700 Aquivion™, 10 % ZrP nanofibres	80	50	39
		90	140
	110	50	33
		90	126

P-O-H of the zirconium hydrogenphosphate. The position of this
[55] peak at -21.8 ppm is that of amorphous ZrP rather than crystalline ZrP, as has been reported Q^3 phosphate[23]. The existence of the shoulder peaks at -15 and -29 ppm can be attributed to phosphates with different coordination of Q^2 and Q^4 respectively[24]. This effect of acid treatment has also been
[60] confirmed by refluxing the ZrP fibres in HCl rather than H_3PO_4 to ensure that the ZrP formation is not due to H_3PO_4 (See Supporting Information), as the ^{31}P NMR spectra of samples treated with H_3PO_4 and HCl were very similar, indicating a similar ZrP composition although the H_3PO_4 treated sample did
[65] show a greater amount of lower-coordinated species which may have been formed during the acid treatment.

Composite membrane of a low EW PFSA and ZrP/ZrO$_2$ nanofibres

Composite membrane containing 5 wt % ZrP/ZrO$_2$ nanofibres
[70] was successfully fabricated by solution casting in a dispersion of Aquivion™, a short-side chain perfluorosulfonic acid polymer. The membranes were cloudy in appearance rather than transparent, but without any visible aggregation.

[75] In-plane proton conductivity measurements of the composite membrane (Table 2) shows that the composite membrane exhibits higher proton conductivity compared to unmodified, cast Aquivion™ membranes of the same equivalent weight (700). This seems to indicate that the presence of the ZrP fibres may
[80] induce some ordering in the ionic domains, in that they may have better interconnectivity due to the Aquivion™-ZrP interface along the fibres. However, increasing the ZrP content of the membrane from 5 to 10 % resulted in a lowered overall conductivity due to the reduced Aquivion™ volume fraction,
[85] although the proton conductivity remains above that of the unmodified membrane.

The composite membrane also shows better performance compared to commercial, EW790 Aquivion™ membrane (which
[90] is made by extrusion) also at higher temperature and lower relative humidity, which indicates improved water retention in the composite membrane. As can be seen in Table 3, under ambient conditions the composite membrane shows an increase in modulus but a similar yield point as commercial Aquivion™,
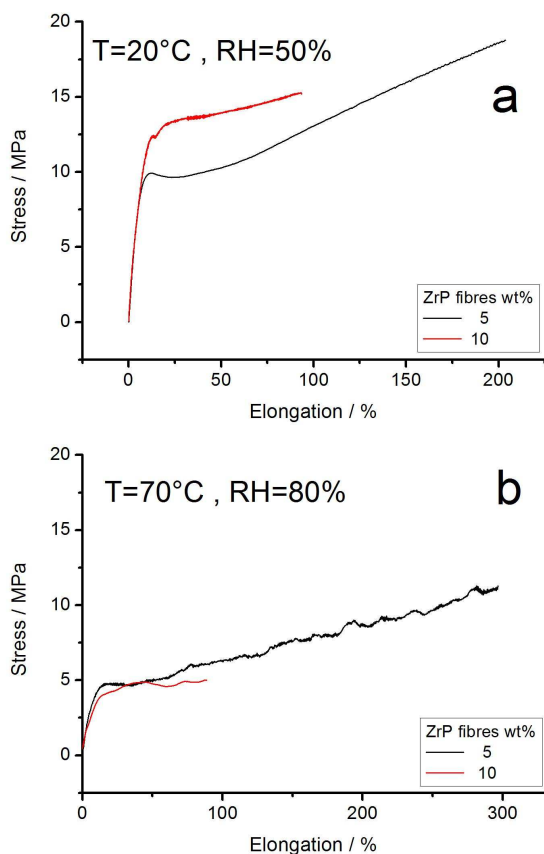[95] with a lowered breaking strength due to the significantly lower

Fig. 5 Mechanical stress-strain measurement of the composite membranes at (a) ambient temperature and RH, and (b) 70 °C and 80 % RH

Table 3 Mechanical properties of the composite membranes compared to reference membranes; E_{mod}: Elastic Modulus δ_y: Yield Point; δ_b: Breaking Strength El: Elongation at Break

Membrane Sample	T (°C)	RH (%)	E_{mod} (Mpa)	δ_y (MPa)	δ_b (MPa)	El (%)
Commercial, extruded EW790 Aquivion™	20	50	149	10.8	36	450
	70	80	48	5.1	16	557
Cast EW700 Aquivion™	20	50	125	10.1	21	309
	70	80	40	3.9	13	315
Cast EW700 Aquivion™, 5% ZrP nanofibres	20	50	175	10	16	172
	70	80	73	4.4	9.2	231
Cast EW700 Aquivion™, 10% ZrP nanofibres	20	50	208	11.8	14.6	94
	70	80	40	2.2	3.9	95

elongation at break. However, at 70 °C and 80 % RH the difference increased significantly with an elastic modulus of 73 MPa for the composite membrane compared to 48 MPa for commercial Aquivion™. Under this conditions, which may be expected in an operating fuel cell, the composite membrane with 5 % ZrP demonstrates a greater elastic modulus and yield point compared to the reference membranes, which may be expected to improve the membrane's resistance to deformation such as creep, which may reduce the membrane thickness and thus increase the possibility of membrane failure.

Increasing the ZrP fibre content from 5 % to 10 % resulted in increased mechanical properties under ambient conditions, however when the temperature and humidity were increased the membrane containing 10 % ZrP fibres show a larger decrease in mechanical properties, resulting in similar elastic modulus and lower yield point for the sample with 10 % ZrP. The membrane with 10 % ZrP also show a much shorter elongation at break, resulting in lowered breaking strength. This indicates that the plasticity of these composite membranes depends mostly on the Aquivion™ content, and a very high ZrP content is detrimental rather than beneficial to the overall mechanical integrity of the membrane.

Unfortunately, a direct comparison between membranes based on EW 700 Aquivion containing ZP fibres and ZP nanoparticles is not possible since the latter has not been reported in the literature. Nevertheless, we can compare the proportional changes in the conductivity and mechanical properties of EW 700 Aquivion induced by the ZP fibres with the corresponding proportional changes in the properties of EW 830 Aquivion due to ZP nanoparticles of low aspect ratio[26]. The proportional increase in the Young's modulus of the composite membrane, with respect to the Young's modulus of the neat ionomer, is higher for the membranes filled with ZrP fibres than for the corresponding membranes filled with ZP nanoparticles; as an example, the proportional increase in the Young's modulus for the composites filled with 5 wt% of ZP fibres and nanoparticles is 40% and 27%, respectively, at ambient conditions. This effect becomes more significant at higher temperature and relative humidity: at 70°C – 80% RH, the proportional increase in the Young's modulus for an EW 700 Aquivion membrane filled with 5 wt% ZP fibres is 83%, while the corresponding increase for an EW 830 Aquivion membrane loaded with 5 wt% ZP nanoparticles is only 5%. Moreover, while the conductivity of EW 700 Aquivion loaded with 5 wt% fibres benefits from the presence of the filler (being up to 27% higher than that of EW 700 Aquivion, at 110 °C – 90% RH), the composite membranes filled with the same amount of ZP nanoparticles are less conductive than the neat ionomer, by about 20%, in the temperature range from 90 to 120°C, both at 50% and 90% RH.

Conclusions

Zirconium phosphate/zirconium oxide composite fibres have been prepared by electrospinning using a novel, reactive coaxial electrospinning approach where a coaxial needle was used to prevent premature mixing and gelation of the reactants. The use of a coaxial needle to separate the solutions of the zirconium precursor and phosphorus source prevents gelation due to the formation of ZrP gel and enables fibre formation. Calcination and H_3PO_4 treatment of these fibres yield the ZrP/ZrO$_2$ nanofibres, the formation of which was confirmed using ^{31}P NMR. The fibre morphology is dependent on solution parameters such as the concentration of the phosphorus source, which suggests that the fibre diameter is dependent on the gelling time of the solution. Cross-section HRTEM EDS shows equal concentration of phosphorus on the edge and centre of the fibres, indicating that its

formation was sufficiently rapid, resulting in an amorphous rather than core-shell morphology. Incorporation of the nanofibres into Aquivion™ (a short-side chain perfluorosulfonic acid) membranes resulted in increased mechanical properties with greater elastic modulus and yield point as well as increased proton conductivity compared to both cast and commercial Aquivion™ membrane, showing the potential of such nanofibre reinforced membrane in fuel cell applications.

Acknowledgements

Notes and references

^{a} *Institute Charles Gerhardt Montpellier, UMR CNRS 5253, Agrégats, Interfaces et Matériaux pour l'Energie, Université Montpellier 2, Place Eugène Bataillon, 34095 Montpellier cédex 5, France.*
^{b} *Dipartimento di Chimica, Università degli Studi di Perugia,Via Elce di Sotto 8, Perugia, Italy*
Corresponding author: surya.subianto@univ-montp2.fr ; deborah.jones@univ-montp2.fr

† Electronic Supplementary Information (ESI) available: WDS and XRD Spectra of the ZrP/ZrO$_2$ fibres, solid state ^{31}P NMR spectra comparison of calcined ZrP/ZrO$_2$ fibres treated with H$_3$PO$_4$ and HCl.See DOI: 10.1039/b000000x/

1. M. Casciola, G. Bagnasco, A. Donnadio, L. Micoli, M. Pica, M. Sganappa and M. Turco, *Fuel Cells*, 2009, **9**, 394-400.
2. M. Casciola, D. Capitani, A. Comite, A. Donnadio, V. Frittella, M. Pica, M. Sganappa and A. Varzi, *Fuel Cells*, 2008, **8**, 217-224.
3. P. Costamagna, C. Yang, A. B. Bocarsly and S. Srinivasan, *Electrochimica Acta*, 2002, **47**, 1023-1033.
4. C. Yang, S. Srinivasan, A. B. Bocarsly, S. Tulyani and J. B. Benziger, *Journal of Membrane Science*, 2004, **237**, 145-161.
5. G. Alberti, M. Casciola, D. Capitani, a. Donnadio, R. Narducci, M. Pica and M. Sganappa, *Electrochimica Acta*, 2007, **52**, 8125-8132.
6. M. Casciola, D. Capitani, A. Donnadio, V. Frittella, M. Pica and M. Sganappa, *Fuel Cells*, 2009, **9**, 381-386.
7. Y.-P. Fang, A.-W. Xu, R.-Q. Song, H.-X. Zhang, L.-P. You, J. C. Yu and H.-Q. Liu, *Journal of the American Chemical Society*, 2003, **125**, 16025-16034.
8. S. Subianto, M. Pica, M. Casciola, P. Cojocaru, L. Merlo, D. J. Jones and G. Hards, *Journal of Power Sources*, 2013, **233**, 216-230.
9. S. Cavaliere, S. Subianto, I. Savych, D. J. Jones and J. Roziere, *Energy Environmental Science*, 2011, **4**, 4761-4785.
10. P. Barboux and J. Livage, *Solid State Ionics*, 1989, **34**, 47-52.
11. M. Casciola, U. Costantino and S. D'amico, *Solid State Ionics*, 1988, **28-30, part 1**, 617-621.
12. A. Goni Urtiaga, K. Scott, S. Cavaliere, D. J. Jones and J. Roziere, *Journal of Materials Chemistry A*, 2013, **1**, 10875-10880.
13. C. Wessel, R. Ostermann, R. Dersch and B. M. Smarsly, *Journal of Physical Chemistry C*, 2011, **115**, 362-372.
14. S. Cavaliere, S. Subianto, L. Chevallier, D. J. Jones and J. Rozière, *Chemical communications*, 2011, **47**, 6834-6836.
15. A.-M. Azad, T. Matthews and J. Swary, *Materials Science and Engineering B*, 2005, **123**, 252-258.
16. C. Shao, H. Guan, Y. Liu, J. Gong, N. Yu and X. Yang, *Journal of Crystal growth*, 2004, **267**, 380-384.
17. E. Davies, A. Lowe, M. Sterns, K. Fujihara and S. Ramakhrisna, *Journal of the American Ceramic Society*, 2008, **91**, 1115-1120.
18. D. Carriere, M. Moreau, P. Barboux, J.-P. Boilot and O. Spalla, *Langmuir : the ACS Journal of Surfaces and Colloids*, 2004, **20**, 3449-3455.
19. D. Carriere, M. Moreau, K. Lhalil, P. Barboux and J. P. Boilot, *Solid State Ionics*, 2003, **162-163**, 185-190.
20. S. B. Randarevich, V. V. Strelko, V. N. Belyakov and A. I. Bortun, *Theoretical and Experimental Chemistry*, 1989, **24**, 607-610.
21. D. G. Yu, C. Branford-White, K. White, N. P. Chatterton, L.-M. Zhu, L. Y. Huang and B. Wang, *Express Polymer Letters*, 2011, **5**, 732-741.
22. D.-G. Yu, C. Branford-White, S. W. A. Bligh, K. White, N. P. Chatterton and L.-M. Zhu, *Macromolecular Rapid Communications*, 2011, **32**, 744-750.
23. J. Chabe, M. Bardet and G. Gebel, *Solid State Ionics*, 2012, **229**, 20-25.
24. M. J. Hudson, A. D. Workman and R. J. W. Adams, *Solid State Ionics*, 1991, **46**, 159-165.
25. J.-H. Jung and H.-J. Sohn, *Microporous and Mesoporous Materials*, 2007, **106**, 49-55.
26. M. Pica, A. Donnadio, M. Casciola, P. Cojocaru and L. Merlo, *Journal of Materials Chemistry*, 2012, **22**, 24902-24908.

Reactive Coaxial Electrospinning of ZrP/ZrO$_2$ Nanofibres

S. Subianto[a], A. Donnadio[b], S. Cavaliere[a], M. Pica[b], M. Casciola[b], D. J. Jones[a], and J. Rozière[a]
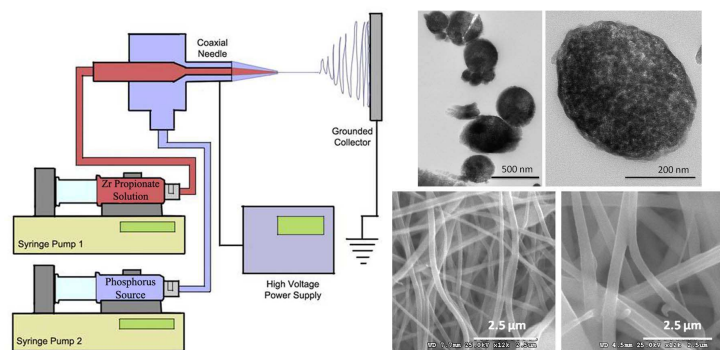
Zirconium phosphate/zirconium oxide nanofibres have been fabricated using a novel, reactive coaxial electrospinning approach where a zirconium precursor and a phosphorus source are spun together from separate solutions using a coaxial needle.